Nonlinear pulse propagation in twin-core-fiber rocking filters

W. E. P. Padden
School of Physics, University of Sydney, New South Wales 2006, Australia

C. Martijn de Sterke and D. C. Psaila
School of Physics, and Optical Fibre Technology Centre, University of Sydney, New South Wales 2006, Australia
(Received 22 March 1995)

Nonlinear pulse propagation is investigated in a twin-core, birefringent rocking filter, a structure for which the linear properties indicate the presence of two stop gaps. It is found that in two special cases, the four nonlinear, coupled-mode equations that describe the system can be reduced to a pair of equations that have been well studied. Consequently, two kinds of compound solitary waves are obtained, which are generalizations of previous results: one that propagates down the structure with equal power in each core and a solution that periodically couples completely from core to core without degradation.

PACS number(s): 42.81.Dp, 42.65.Re, 42.81.Gs

I. INTRODUCTION

In a single-mode birefringent fiber, light launched along a principal polarization axis maintains that polarization state. In this paper, an in-line birefringent fiber rocking filter is considered, which is a structure that rotates the polarization state of the optical field. To achieve this, the fiber's principal axes are periodically rocked through a small angle, either by oscillating the fiber preform during the drawing process [1] or by using uv light [2] to externally irradiate the fiber periodically. Since the birefringence beat length is wavelength dependent, there is a resonant wavelength at which the beat length is equal to the rocking filter twisting period. At this wavelength there is complete coupling from one polarization mode to the other, while at other wavelengths there is only partial coupling. As such, the power conversion between the two orthogonally polarized modes is wavelength dependent (see [1] for details of the operation of a rocking filter).

Wabnitz [3] studied the effects of a Kerr nonlinearity on group-velocity dispersion-free propagation of two orthogonally polarized, copropagating pulses in a resonant fiber rocking filter. He found that, even though the material dispersion is assumed negligible, there exist novel solitary wave solutions, resonance solitons, in which nonlinearity balances the dispersion due to the different group velocities of the two linearly coupled modes. Resonance solitons are vector solitons, containing both polarizations, which resist walkoff due to the different group velocities.

Recently, Psaila and de Sterke (hereafter referred to as PdS) [4] extended the analysis of Wabnitz by including a second birefringent, fiber rocking filter core. The two cores are assumed to be identical, so that the propagation constants along each polarization axis are equivalent. They also take the orientation of both cores such that the principal axes are aligned along the x and y directions. Hence, any coupling between orthogonally polarized modes of different cores is neglected. They found that the system of four nonlinear, coupled-mode equations can be reduced to a pair of coupled nonlinear Schrödinger equations under suitable approximations. The authors found two new types of four-component solitons: one solution propagates simultaneously down both cores with equal power in all four components and the other solution periodically couples both polarization modes completely from core to core. A directional coupler exhibits similar behavior; however, there is only one mode present in each core. It was shown in numerical simulations of the original nonlinear coupled-mode equations that both types of solitons can propagate for thousands of core-to-core couplings without appreciable change in the pulse shape.

The solutions obtained by PdS are only valid for solitons with small amplitude and with a velocity close to the average group velocity of the two orthogonal polarizations. As will be explained more fully in Sec. II, these solutions correspond to a pulse center wave vector just inside the photonic stop gap. It is also indicated that in this work the term gap means that evanescent field solutions exist in a certain region of frequency–wave-vector space. Also, note that stop gaps are not unique to rocking filters but are a feature of any periodic structure [5]. In the present paper, the results of PdS are generalized by obtaining exact analytic solutions to the coupled-mode equations themselves, without taking the limit where the nonlinear Schrödinger equations are valid. These four-component solutions are shown to be valid for pulse center wave vectors anywhere in the stop gap, not just close to the gap edge. These solutions are thus valid for much larger pulse amplitudes and represent high-power generalizations of those obtained by PdS.

The layout of this paper is as follows. In Sec. II the coupled-mode equations are presented and the properties of the linearized equations are analyzed to determine the gap structure of the system. As will be shown, in general there are two stop gaps and it is important to identify exactly in which stop gap the center wave vector of the pulse lies. In Sec. III, analytic solutions are obtained for the nonlinear coupled-mode equations in two special

cases. Numerical simulations of the two types of solutions propagating down the twin-core rocking filter are also presented in this section. In Sec. IV the question of the stability of the solutions to certain perturbations is discussed. Finally the results are discussed and conclusions presented in Sec. V.

II. COUPLED-MODE EQUATIONS

In this section the coupled-mode equations for the twin-core, birefringent, resonant fiber rocking filter are presented and the linear properties of the system are determined. It is assumed that the two birefringent cores are identical so that the propagation constants along each polarization axis for each core are equal. Thus, taking the principal axes to be along the x and y directions, we have $\beta_{1x} = \beta_{2x} = \beta_x$ and $\beta_{1y} = \beta_{2y} = \beta_y$, where the subscripts 1 and 2 indicate the two cores. This allows one to neglect any coupling between orthogonally polarized modes of different cores. The total electric field propagating in the structure is written as

$$\mathbf{E}(\mathbf{r},z,t) = \{[A_{1x}(z,t)\mathcal{E}_{1x}(\mathbf{r}) + A_{2x}(z,t)\mathcal{E}_{2x}(\mathbf{r})]\exp(i\beta_x z)\hat{\mathbf{x}} + [A_{1y}(z,t)\mathcal{E}_{1y}(\mathbf{r}) + A_{2y}(z,t)\mathcal{E}_{2y}(\mathbf{r})]\exp(i\beta_y z)\hat{\mathbf{y}}\}\exp(-i\omega t) + \text{c.c.}, \quad (1)$$

where ω is the mean optical frequency, the $\mathcal{E}_{nj}$ (where $n = 1, 2$ and $j = x, y$) are the transverse modal field distributions, $A_{nj}(z,t)$ denotes the slowly varying complex amplitudes of the four polarization modes, $\hat{\mathbf{x}}$, and $\hat{\mathbf{y}}$ are orthogonal unit vectors, and c.c. denotes the complex conjugate.

To obtain evolution equations for the complex envelopes $A_{nj}(z,t)$, the electric field in Eq. (1) is substituted into the wave equation. Assuming a nonlinear Kerr medium and that the cores are sufficiently separated so that any mutual nonlinear interaction can be ignored, the envelopes satisfy the coupled-mode equations (see, e.g., [4, 6–8])

$$i\frac{\partial A_{nx}}{\partial z} + \frac{i}{V_x}\frac{\partial A_{nx}}{\partial t} + \kappa_g A_{ny}\exp(-2i\nu z) + \kappa_c A_{3-nx} + \left(\Gamma_a|A_{nx}|^2 + \Gamma_b|A_{ny}|^2\right)A_{nx} = 0,$$

$$i\frac{\partial A_{ny}}{\partial z} + \frac{i}{V_y}\frac{\partial A_{ny}}{\partial t} + \kappa_g A_{nx}\exp(+2i\nu z) + \kappa_c A_{3-ny} + \left(\Gamma_a|A_{ny}|^2 + \Gamma_b|A_{nx}|^2\right)A_{ny} = 0. \quad (2)$$

For the coupled-mode equations in core 1 (2), one puts $n = 1$ (2). In Eqs. (2), the $V_{x,y}$ are the group velocities in each polarization mode; $2\nu = k_x - k_y - 2\pi/L_t$, with L_t the rocking filter twist period, is a detuning. In the case of a resonant fiber rocking filter the twist period is equal to the birefringence beat length L_b and $\nu = 0$; κ_c represents the linear core-to-core coupling; while Γ_a and Γ_b are the self- and cross-phase modulation constants, respectively. Usually it is taken that $\Gamma_a = 3\Gamma_b/2$; however, in this work it is assumed the relationship between Γ_a and Γ_b is completely general. Finally, κ_g is the linear coupling coefficient due to the presence of the rocking filter. This coupling constant depends on the rocking filter twist angle θ and the modal birefringence $\Delta n = |n_x - n_y|$ [8] via

$$\kappa_g = \frac{\Delta n\,\theta\,\omega}{4c} \equiv \frac{\pi\theta}{2L_b}, \quad (3)$$

where c is the speed of light. Equation (3) indicates that the coupling constant scales as the inverse of the beat length, which is to be expected, since at resonance the polarization mode rotates through an angle 2θ per twist period (see [9]). Note that the form of Eq. (2) indicates that material dispersion has been ignored (see [10] for a discussion of the conditions under which this is valid).

Equation (2) can be cast in simpler form if one makes the substitution

$$A_{nj} = \mathcal{R}_{nj}\exp[i\nu\{\mp z + t/d - z/(dV_g)\}], \quad (4)$$

where the upper (lower) sign refers to the $j = x$ (y) polarization and

$$d = \frac{1}{2}(V_x^{-1} - V_y^{-1}), \qquad V_g = \frac{2V_xV_y}{V_x + V_y}, \quad (5)$$

represent the group-velocity mismatch and an average group velocity, respectively. Substituting Eq. (4) in Eq. (2), one obtains

$$i\frac{\partial \mathcal{R}_{nx}}{\partial z} + \frac{i}{V_x}\frac{\partial \mathcal{R}_{nx}}{\partial t} + \kappa_g\mathcal{R}_{ny} + \kappa_c\mathcal{R}_{3-nx} + \left(\Gamma_a|\mathcal{R}_{nx}|^2 + \Gamma_b|\mathcal{R}_{ny}|^2\right)\mathcal{R}_{nx} = 0,$$

$$i\frac{\partial \mathcal{R}_{ny}}{\partial z} + \frac{i}{V_y}\frac{\partial \mathcal{R}_{ny}}{\partial t} + \kappa_g\mathcal{R}_{nx} + \kappa_c\mathcal{R}_{3-ny} + \left(\Gamma_a|\mathcal{R}_{ny}|^2 + \Gamma_b|\mathcal{R}_{nx}|^2\right)\mathcal{R}_{ny} = 0. \quad (6)$$

The analysis presented so far has been in laboratory frame coordinates; however, it has been found to be more convenient to change to a new coordinate frame moving at the average group velocity of the the two orthogonally polarized modes. We introduce the new coordinates

$$\zeta = z, \qquad \tau = \frac{t - z/V_g}{d}, \quad (7)$$

so that τ is a retarded time; then on examining Eq. (4) it is seen that in the new coordinate system it can be rewritten as

$$A_{nj} = \mathcal{F}_{nj}\exp[i\nu(\tau \mp \zeta)], \quad (8)$$

where the upper (lower) sign refers to the $j = x$ (y) polarization mode. In this new coordinate frame, the four coupled-mode equations Eqs. (6) take their final form

$$i\frac{\partial \mathcal{F}_{nx}}{\partial \zeta} + i\frac{\partial \mathcal{F}_{nx}}{\partial \tau} + \kappa_g \mathcal{F}_{ny} + \kappa_c \mathcal{F}_{3-nx} + \left(\Gamma_a|\mathcal{F}_{nx}|^2 + \Gamma_b|\mathcal{F}_{ny}|^2\right)\mathcal{F}_{nx} = 0,$$

$$i\frac{\partial \mathcal{F}_{ny}}{\partial \zeta} - i\frac{\partial \mathcal{F}_{ny}}{\partial \tau} + \kappa_g \mathcal{F}_{nx} + \kappa_c \mathcal{F}_{3-ny} + \left(\Gamma_a|\mathcal{F}_{ny}|^2 + \Gamma_b|\mathcal{F}_{nx}|^2\right)\mathcal{F}_{ny} = 0. \quad (9)$$

In writing down these coupled-mode equations, the x-polarized mode is taken to travel more slowly than the y-polarized mode, i.e., $V_x < V_y$.

Linear properties of coupled-mode equations

Before proceeding further with the nonlinear coupled-mode equations, it is instructive to analyze the properties of the linear system of equations in both the laboratory frame and the new coordinate frame. First, for the laboratory frame, dropping the nonlinear terms in Eqs. (6) one obtains

$$i\frac{\partial \mathcal{R}_{nx}}{\partial z} + \frac{i}{V_x}\frac{\partial \mathcal{R}_{nx}}{\partial t} + \kappa_g \mathcal{R}_{ny} + \kappa_c \mathcal{R}_{3-nx} = 0,$$

$$i\frac{\partial \mathcal{R}_{ny}}{\partial z} + \frac{i}{V_y}\frac{\partial \mathcal{R}_{ny}}{\partial t} + \kappa_g \mathcal{R}_{nx} + \kappa_c \mathcal{R}_{3-ny} = 0. \quad (10)$$

The next step is to find the linear supermodes of the system, to which end the following *Ansatz* is employed:

$$\mathcal{R}_{nj} = S_{nj}\exp[-i(\Omega t - Qz)], \quad (11)$$

where Ω and Q represent the frequency and wave number of the slowly varying envelopes S_{nj}. Inserting Eq. (11) into Eqs. (10) one obtains a set of four algebraic equations for the S_{nj}. For nontrivial solutions the determinant of the matrix of coefficients must vanish; on solving the resulting quartic equation as a function of Ω one obtains four real solutions given by

$$\Omega_{\pm}^{(1)} = \frac{(\kappa_c + Q)(V_x + V_y) \pm \sqrt{(\kappa_c + Q)^2(V_x - V_y)^2 + 4\kappa_g^2 V_x V_y}}{2},$$

$$\Omega_{\pm}^{(2)} = \frac{(-\kappa_c + Q)(V_x + V_y) \pm \sqrt{(-\kappa_c + Q)^2(V_x - V_y)^2 + 4\kappa_g^2 V_x V_y}}{2}, \quad (12)$$

which correspond to the four hyperbolic branches of the dispersion relation in frequency–wave-vector space. In general, the solutions given in Eq. (12) indicate there are two distinct stop gaps. However, unlike the case of contrapropagating modes, where the stop gap is a gap in frequency, in this case there is a gap in frequency and wave vector. The existence of such gaps is well known and is a feature of any system which involves the coupling of copropagating modes (see [11] for a more complete discussion of this issue).

In Fig. 1 are presented plots of the dispersion relations in two parameter regimes: (a) $\kappa_c < \kappa_g$; (b) $\kappa_c > \kappa_g$. The diagram for $\kappa_c = \kappa_g$ is an obvious intermediate case and is not presented. Given that in most practical applications the coupling between cores is on a scale of order millimeters, while the coupling between polarization modes is on a scale of order a meter, then $\kappa_c \gg \kappa_g$. Hence, it is the diagram of Fig. 1(b) which is of most relevance in this work. It is usually understood that a gap is a region without running wave solutions. Strictly, therefore, the diagrams in Fig. 1 indicate there are no such regions. But, in this paper, it is understood that a gap is a region in which evanescent waves occur, as in the regions highlighted by the double bold arrows in Fig. 1. In this case there are two distinct stop gaps.

The soliton solutions obtained by PdS in their Eq. (10) correspond to modes with a wave vector $Q \gtrsim \kappa_c - \kappa_g$ and thus in order to make contact with these solutions it is modes with wave vectors in the range $\kappa_c - \kappa_g < Q < \kappa_c + \kappa_g$ that need to be considered. The solutions given in Eq. (12) of PdS actually involve wave vectors $Q \gtrsim \pm\kappa_c - \kappa_g$, i.e., from both gap regions shown in Fig. 1(b). Further discussion of these ideas is given in Sec. V.

Now consider the new coordinate frame and contrast the results to those obtained above. The linearized version of Eq. (9) is

$$i\frac{\partial \mathcal{F}_{nx}}{\partial \zeta} + i\frac{\partial \mathcal{F}_{nx}}{\partial \tau} + \kappa_g \mathcal{F}_{ny} + \kappa_c \mathcal{F}_{3-nx} = 0,$$

$$i\frac{\partial \mathcal{F}_{ny}}{\partial \zeta} - i\frac{\partial \mathcal{F}_{ny}}{\partial \tau} + \kappa_g \mathcal{F}_{nx} + \kappa_c \mathcal{F}_{3-ny} = 0. \quad (13)$$

We make the *Ansatz*

$$\hat{\mathcal{F}} = \hat{G}\exp[-i(\Omega'\tau - Q'\zeta)], \quad (14)$$

where the notation $\hat{\mathcal{F}}$ indicates a vector with four components; $\mathcal{F}_{1x}$, $\mathcal{F}_{1y}$, $\mathcal{F}_{2x}$, and $\mathcal{F}_{2y}$, and similarly for $\hat{G}$. Also the G_{nj} do not depend on τ or ζ. Using Eq. (14) in Eq. (13) one obtains a set of algebraic equations for the G_{nj} which lead to the set of dispersion relations

$$Q_{\pm}'^{(1)} = \kappa_c \pm \sqrt{\Omega'^2 + \kappa_g^2},$$

$$Q_{\pm}'^{(2)} = -\kappa_c \pm \sqrt{\Omega'^2 + \kappa_g^2}. \quad (15)$$

Introducing the Dirac ket $|m\rangle$ notation to denote the linear supermodes, then in the limit $\Omega' = 0$, which is the region of interest in this work, the supermodes corresponding to the eigenvalues in Eqs. (15) attain the simple form

$$|1\rangle = \begin{pmatrix} 1 \\ -1 \\ 1 \\ -1 \end{pmatrix}, \quad |2\rangle = \begin{pmatrix} 1 \\ 1 \\ 1 \\ 1 \end{pmatrix},$$

$$|3\rangle = \begin{pmatrix} 1 \\ -1 \\ -1 \\ 1 \end{pmatrix}, \quad |4\rangle = \begin{pmatrix} 1 \\ 1 \\ -1 \\ -1 \end{pmatrix}, \tag{16}$$

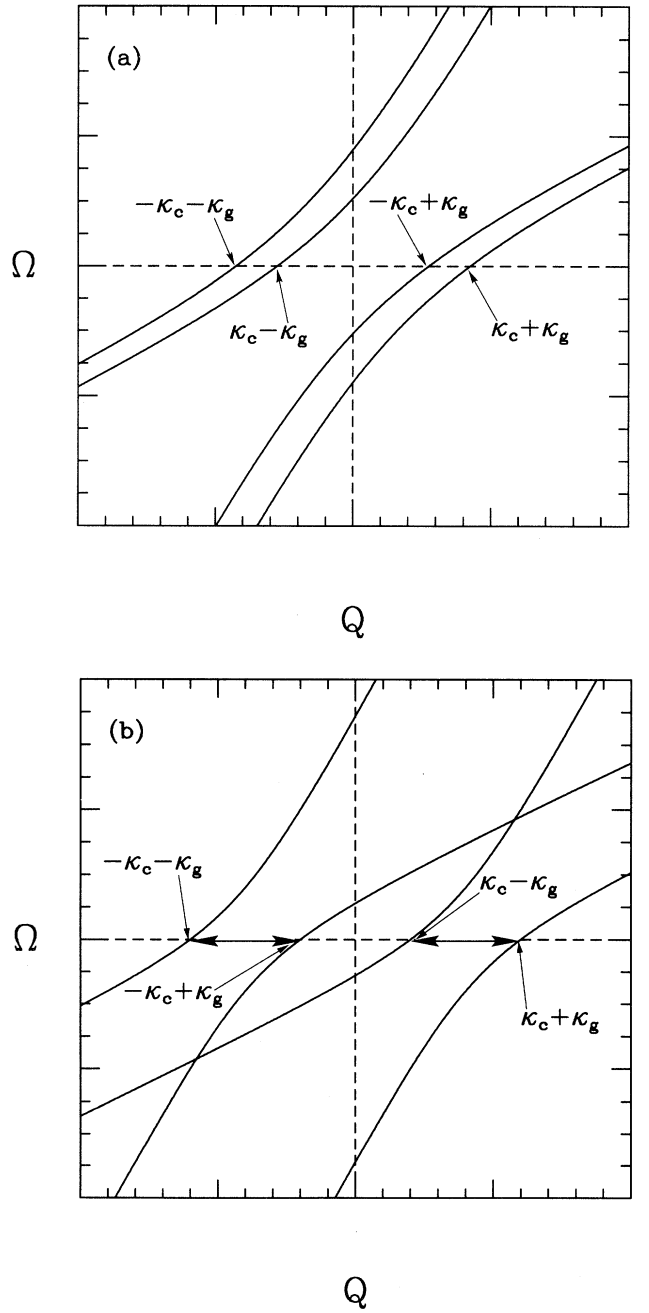

FIG. 1. Diagram showing the stop gap structure of the dispersion relation for a twin-core-fiber rocking filter in two parameter regimes: (a) $\kappa_c < \kappa_g$; (b) $\kappa_c > \kappa_g$. The bold double-headed arrows in (b) indicate the wave vectors of the solutions of interest.

while the eigenvalues reduce to $Q'^{(1)}_{\pm} = \kappa_c \pm \kappa_g$ and $Q'^{(2)}_{\pm} = -\kappa_c \pm \kappa_g$. Henceforth, it is understood that all results in this paper pertain to the special case $\Omega' = 0$.

In Fig. 2 is shown a plot of the dispersion relations for the parameter regimes (a) $\kappa_c > \kappa_g$; (b) $\kappa_c > \kappa_g$. In this new coordinate frame the dispersion curves have been rotated counterclockwise compared to those in the

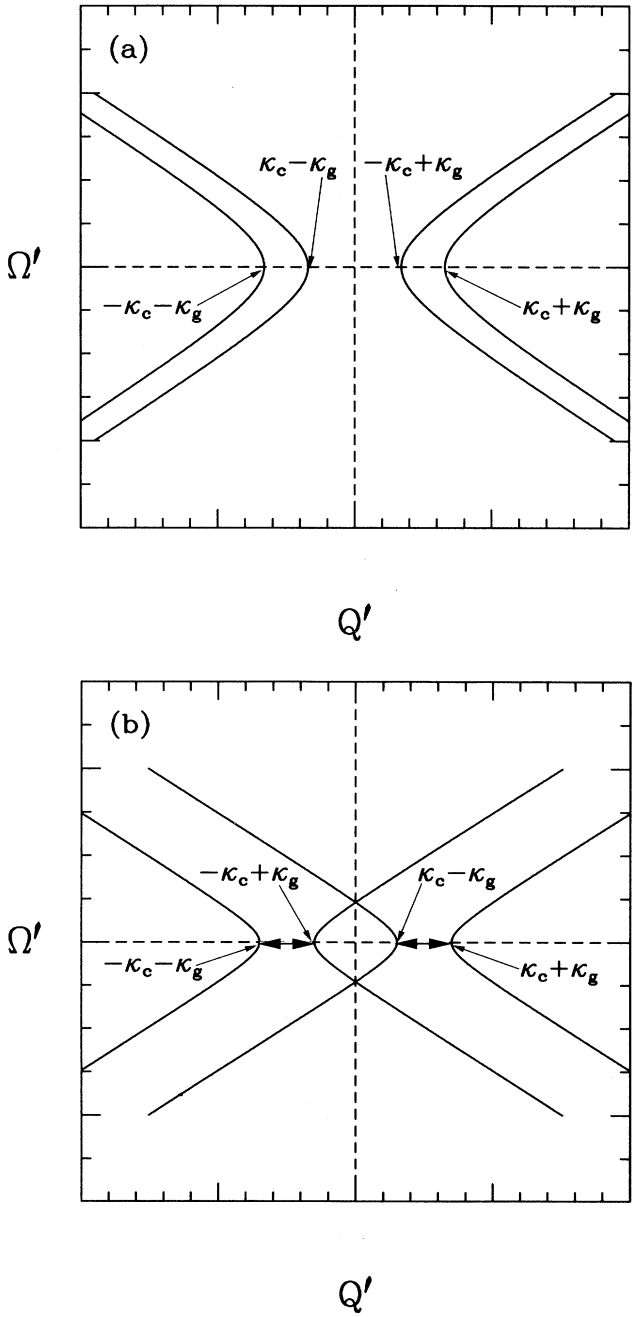

FIG. 2. Diagram showing the stop gap structure of the dispersion relations for a twin-core-fiber rocking filter in the parameter regimes (a) $\kappa_c < \kappa_g$ and (b) $\kappa_c > \kappa_g$, in the coordinate system defined by Eq. (7). The bold double-headed arrows in (b) indicate the wave vectors of the solutions of interest.

laboratory frame and the dispersion curves have sheared as they have rotated. The key point to note here is that the stop gaps are now purely a wave vector gap.

III. SOLUTIONS OF COUPLED-MODE EQUATIONS

As mentioned earlier, the aim of this paper is to find a generalization of the solutions of PdS beyond the nonlinear Schrödinger limit, such that they are valid anywhere in the stop gap, not just near the gap edge, and have velocity anywhere between V_x and V_y. In the Introduction it was indicated that PdS obtained two classes of four-component solution: one solution propagates simultaneously down both cores with equal power in all four components and the other solution periodically couples completely from core to core. Hence, using the PdS solutions for guidance, the nonlinear coupled-mode equations [Eqs. (9)] are analyzed in two special cases. In Sec. III A solutions are obtained in which the x-polarized modes of each core have the same power and similarly for the y-polarized modes of each core. In Sec. III B solutions are presented which periodically couple from core to core.

A. Solutions with equal power in each core

As Eqs. (9) stand, it is not known whether they integrable and to find exact analytic solutions in general, would be difficult. The number of possible solutions can be restricted considerably by examining the form of the solution of PdS which has equal power in all four modes. This suggests that the nonlinear coupled-mode equations be reduced by making the assumption

$$\mathcal{F}_{1x} = \mathcal{F}_{2x} = \mathcal{F}_x, \qquad \mathcal{F}_{1y} = \mathcal{F}_{2y} = \mathcal{F}_y. \tag{17}$$

See Sec. IV for a discussion of the *Ansatz*. Substituting Eq. (17) into Eqs. (9) one finds the following system of nonlinear coupled equations:

$$i\frac{\partial \mathcal{F}_x}{\partial \zeta} + i\frac{\partial \mathcal{F}_x}{\partial \tau} + \kappa_g \mathcal{F}_y + \kappa_c \mathcal{F}_x + \left(\Gamma_a|\mathcal{F}_x|^2 + \Gamma_b|\mathcal{F}_y|^2\right)\mathcal{F}_x = 0,$$

$$i\frac{\partial \mathcal{F}_y}{\partial \zeta} - i\frac{\partial \mathcal{F}_y}{\partial \tau} + \kappa_g \mathcal{F}_x + \kappa_c \mathcal{F}_y + \left(\Gamma_a|\mathcal{F}_y|^2 + \Gamma_b|\mathcal{F}_x|^2\right)\mathcal{F}_y = 0. \tag{18}$$

The terms proportional to κ_c in Eq. (18) are just self-coupling terms and can be removed by the simple transformation

$$\mathcal{F}_{x,y} = F_{x,y} e^{i\kappa_c \zeta}, \tag{19}$$

which leads to the final form for the two nonlinear coupled-mode equations:

$$i\frac{\partial F_x}{\partial \zeta} + i\frac{\partial F_x}{\partial \tau} + \kappa_g F_y + \left(\Gamma_a|F_x|^2 + \Gamma_b|F_y|^2\right)F_x = 0,$$
$$i\frac{\partial F_y}{\partial \zeta} - i\frac{\partial F_y}{\partial \tau} + \kappa_g F_x + \left(\Gamma_a|F_y|^2 + \Gamma_b|F_x|^2\right)F_y = 0. \tag{20}$$

It is seen that Eqs. (20) are identical to those for a single-core birefringent fiber rocking filter. Equations (20) are in general nonintegrable and thus soliton solutions do not exist. Aceves and Wabnitz [12] found solitary wave solutions to the coupled-mode equations for contrapropagating modes in a nonlinear periodic medium. The solutions of [12] can be adapted to Eqs. (20) by simply interchanging the roles of space and time, which leads to the following results (here the notation of de Sterke and Sipe [7] is employed):

$$F_{x,y} = \alpha \mathcal{G}_{x,y} e^{i\eta(\theta)}, \tag{21}$$

where $\mathcal{G}_{x,y}$ denote the solutions to the massive Thirring model (see [12] for details), which are given by

$$\mathcal{G}_x = \sqrt{\frac{\kappa_g}{\Gamma_b}}\frac{1}{\Delta}\sin(\delta)e^{i\sigma}\operatorname{sech}(\theta - i\delta/2),$$
$$\mathcal{G}_y = -\sqrt{\frac{\kappa_g}{\Gamma_b}}\Delta\sin(\delta)e^{i\sigma}\operatorname{sech}(\theta + i\delta/2). \tag{22}$$

These solutions assume that the fiber rocking filter has positive nonlinearity and that κ_g is also positive. Further, one has

$$\theta = \gamma\kappa_g(\tau - q\zeta)\sin(\delta), \qquad \sigma = \gamma\kappa_g(q\tau - \zeta)\cos(\delta), \tag{23}$$

where the dimensionless quantities q and γ are given by

$$q = \frac{1-\Delta^4}{1+\Delta^4}, \qquad \gamma = \frac{1}{\sqrt{1-q^2}}; \tag{24}$$

thus γ is the Lorentz factor. The final definitions are

$$\alpha = (1 + R_+ + R_-)^{-1/2}, \tag{25}$$

and

$$e^{i\eta(\theta)} = \left[-\frac{e^{2\theta} + e^{-i\delta}}{e^{2\theta} + e^{i\delta}}\right]^{(R_+ - R_-)/(1+R_+ + R_-)}, \tag{26}$$

with

$$R_\pm = \frac{\Gamma_a}{2\Gamma_b}\frac{(1\pm q)^2}{1-q^2}. \tag{27}$$

It is seen from Eqs. (22) and Eq. (23) that these solutions are characterized by two parameters: $0 < \delta < \pi$ and $-1 < q < 1$. According to Eq. (23) and Eq. (24), q (and thus Δ) determine the soliton's velocity, while δ determines the position in the stop gap. Referring to Fig. 1(b), the value $\delta \to 0$ denotes a solution with center wave vector near $\kappa_c - \kappa_g$, corresponding to a wide, low-amplitude pulse (the low-intensity limit), while $\delta \to \pi$ would correspond to a solution with center wave vector near $\kappa_c + \kappa_g$, corresponding to a narrow, large-amplitude pulse (the high-intensity limit). The solitary wave travels with a velocity

$$V_g(q) = \frac{2V_xV_y}{V_x(1-q) + V_y(1+q)} \tag{28}$$

in the laboratory frame, which takes on any value be-

tween V_x and V_y [cf. Eq. (5)]. Note that Aceves and Wabnitz [12] have verified by numerical simulation that the solutions Eqs. (21)–(27) do not have all the properties commonly required of solitons and are thus strictly solitary waves.

Finally then, using Eq. (19) and Eqs. (21)–(27), the complete solution to the coupled-mode equations [Eqs. (9)] is given by

$$\hat{\mathcal{F}}(\zeta,\tau) = \begin{pmatrix} F_x \\ F_y \\ F_x \\ F_y \end{pmatrix} e^{i\kappa_c\zeta}. \tag{29}$$

There are some important points to note about Eqs. (29): First, this represents an *exact* solution of the coupled-mode equations given in Eq. (9). No approximations were made in deriving this result. Second, Eq. (29) represents a four-component solitary wave that has equal power in each core and propagates as one through the rocking filter structure. It is the generalization of the result obtained by PdS in their Eq. (10) to pulses with wave vector lying anywhere in the stop gap delimited by $\kappa_c - \kappa_g < Q' < \kappa_c + \kappa_g$ (see Sec. V for details of this) and with any velocity between V_x and V_y.

Another important point to note concerns solutions which have very small detunings δ and velocities q. It has been shown by de Sterke and Sipe [7] that in this limit the solutions reduce to the solutions given by the nonlinear Schrödinger equation. In this limit the solutions are dominated by the $|1\rangle$ linear supermode [see Eq. (16)]. Hence this confirms that the solution given by Eq. (29) represents high-power generalizations of those obtained by PdS.

Numerical simulations solving the four coupled-mode equations [Eqs. (9)] which confirm the analytic results are now discussed using the fields given in Eq. (29) along with Eq. (21) as input to the fiber structure. The equations are solved numerically using a generalization of the fourth-order collocation method described by [13].

In these simulations the core-to-core coupling is taken to be $\kappa_c = 10\kappa_g$, although in this case the results are independent of the value of κ_c. The pulses are propagated for 100 core-to-core coupling lengths for different velocity (q) and detuning (δ) parameters. In Fig. 3 is presented an example of one of the simulations using Eq. (29) as input to Eqs. (9). It is clearly seen that the input and output intensities for each polarization mode in each core are the same. Figure 3 shows a pulse for which the velocity (q) is nonzero; in this case the output pulse (centered at $\tau = 5$) is in advance of the position it would have with $q = 0$. The asymmetry between the polarization modes is clearly evident in the figure. This behavior is readily ascertained from Eqs. (22), where it is seen that as $q \to 1$ the amplitude of the x-polarized mode increases, while that of the y-polarized mode decreases, and vice versa in the limit $q \to -1$.

B. Solutions which couple from core to core

In this section solutions are obtained in which both polarization modes of a particular core *completely* couple back and forth from core to core. On examination of Eq. (12) of PdS, which corresponds to the solution which couples from core to core on a length scale κ_c^{-1}, it is seen that the linear combinations

$$\mathcal{F}_{1x} \pm \mathcal{F}_{2x}, \qquad \mathcal{F}_{1y} \pm \mathcal{F}_{2y}, \tag{30}$$

are stationary in ζ. Hence, this implies the coupled-mode equations should be rewritten in terms of the new variables

$$\begin{aligned} \mathcal{L}_1 &= \mathcal{F}_{1x} + \mathcal{F}_{2x}, \qquad \mathcal{L}_2 = \mathcal{F}_{1x} - \mathcal{F}_{2x}, \\ \mathcal{L}_3 &= \mathcal{F}_{1y} + \mathcal{F}_{2y}, \qquad \mathcal{L}_4 = \mathcal{F}_{1y} - \mathcal{F}_{2y}. \end{aligned} \tag{31}$$

In terms of these variables, Eqs. (9) become

$$\begin{aligned}
&i\frac{\partial\mathcal{L}_1}{\partial\zeta} + i\frac{\partial\mathcal{L}_1}{\partial\tau} + \kappa_g\mathcal{L}_3 + \kappa_c\mathcal{L}_1 + \frac{1}{4}[\Gamma_a(|\mathcal{L}_1|^2\mathcal{L}_1 + 2|\mathcal{L}_2|^2\mathcal{L}_1 + \mathcal{L}_2^2\mathcal{L}_1^*) + \Gamma_b\{(|\mathcal{L}_3|^2 + |\mathcal{L}_4|^2)\mathcal{L}_1 + (\mathcal{L}_3^*\mathcal{L}_4 + \mathcal{L}_4^*\mathcal{L}_3)\mathcal{L}_2\}] = 0, \\
&i\frac{\partial\mathcal{L}_3}{\partial\zeta} - i\frac{\partial\mathcal{L}_3}{\partial\tau} + \kappa_g\mathcal{L}_1 + \kappa_c\mathcal{L}_3 + \frac{1}{4}[\Gamma_a(|\mathcal{L}_3|^2\mathcal{L}_3 + 2|\mathcal{L}_4|^2\mathcal{L}_3 + \mathcal{L}_4^2\mathcal{L}_3^*) + \Gamma_b\{(|\mathcal{L}_1|^2 + |\mathcal{L}_2|^2)\mathcal{L}_3 + (\mathcal{L}_1^*\mathcal{L}_2 + \mathcal{L}_2^*\mathcal{L}_1)\mathcal{L}_4\}] = 0, \\
&i\frac{\partial\mathcal{L}_2}{\partial\zeta} + i\frac{\partial\mathcal{L}_2}{\partial\tau} + \kappa_g\mathcal{L}_4 - \kappa_c\mathcal{L}_2 + \frac{1}{4}[\Gamma_a(|\mathcal{L}_2|^2\mathcal{L}_2 + 2|\mathcal{L}_1|^2\mathcal{L}_2 + \mathcal{L}_1^2\mathcal{L}_2^*) + \Gamma_b\{(|\mathcal{L}_3|^2 + |\mathcal{L}_4|^2)\mathcal{L}_2 + (\mathcal{L}_3^*\mathcal{L}_4 + \mathcal{L}_4^*\mathcal{L}_3)\mathcal{L}_1\}] = 0, \\
&i\frac{\partial\mathcal{L}_4}{\partial\zeta} - i\frac{\partial\mathcal{L}_4}{\partial\tau} + \kappa_g\mathcal{L}_2 - \kappa_c\mathcal{L}_4 + \frac{1}{4}[\Gamma_a(|\mathcal{L}_4|^2\mathcal{L}_4 + 2|\mathcal{L}_3|^2\mathcal{L}_4 + \mathcal{L}_3^2\mathcal{L}_4^*) + \Gamma_b\{(|\mathcal{L}_1|^2 + |\mathcal{L}_2|^2)\mathcal{L}_4 + (\mathcal{L}_1^*\mathcal{L}_2 + \mathcal{L}_2^*\mathcal{L}_1)\mathcal{L}_3\}] = 0,
\end{aligned} \tag{32}$$

The terms proportional to κ_c represent self-coupling and can be removed by virtue of the transformations

$$\mathcal{L}_{1,3} = L_{1,3}\exp(i\kappa_c\zeta), \qquad \mathcal{L}_{2,4} = L_{2,4}\exp(-i\kappa_c\zeta). \tag{33}$$

On substituting Eq. (33) in Eqs. (32), nonlinear terms proportional to $\exp(\pm 4i\kappa_c\zeta)$ are generated. In order to simplify the analysis it is assumed here, as in PdS, that the two cores of the fiber rocking filter are sufficiently close so that the exponential factors are rapidly varying and those nonlinear terms can be neglected. This leads to the equations

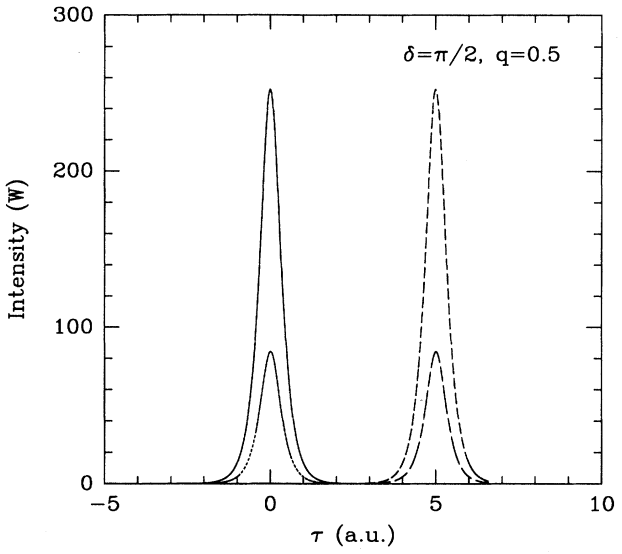

FIG. 3. Numerical simulation of Eqs. (9) using Eq. (29) as input. The key parameters used in the run are shown on the plot. The pulse centered at $\tau = 0$ shows the initial intensity profile of each polarization mode, while the pulse centered at $\tau = 5$ shows the intensity profiles after 100 core-to-core couplings. The units along the τ axis are arbitrary. Other run parameters are: effective modal area 13.6 μm^2, $\lambda = 1.55$ μm, $n_2 = 3.1 \times 10^{-2}$ m^2, W-1, $\kappa_g = \pi/2$ m^{-1}, $\kappa_c = 5\pi$ m^{-1}.

$$i\frac{\partial L_1}{\partial \zeta} + i\frac{\partial L_1}{\partial \tau} + \kappa_g L_3 + \frac{1}{4}\Big[\Gamma_a(|L_1|^2 + 2|L_2|^2)L_1 + \Gamma_b\{(|L_3|^2 + |L_4|^2)L_1 + L_4^* L_3)L_2\}\Big] = 0,$$

$$i\frac{\partial L_3}{\partial \zeta} - i\frac{\partial L_3}{\partial \tau} + \kappa_g L_1 + \frac{1}{4}\Big[\Gamma_a(|L_3|^2 + 2|L_4|^2)L_3 + \Gamma_b\{(|L_1|^2 + |L_2|^2)L_3 + L_2^* L_1)L_4\}\Big] = 0, \quad (34)$$

where the equations for $L_{2,4}$ can be obtained by interchanging the subscripts 1 and 2 as well as the subscripts 3 and 4 in Eqs. (34). Analysis of Eq. (12) of PdS leads one to search for solutions of the form

$$L_1 = L_2, \qquad L_3 = L_4 \quad (35)$$

in Eq. (34). See Sec. IV for a discussion of this *Ansatz*. Equation (35) reduces the system of four coupled nonlinear equations to two coupled nonlinear equations given by

$$i\frac{\partial L_1}{\partial \zeta} + i\frac{\partial L_1}{\partial \tau} + \kappa_g L_3 + \frac{3}{4}\left(\Gamma_a|L_1|^2 + \Gamma_b|L_3|^2\right)L_1 = 0,$$
$$i\frac{\partial L_3}{\partial \zeta} - i\frac{\partial L_3}{\partial \tau} + \kappa_g L_1 + \frac{3}{4}\left(\Gamma_a|L_3|^2 + \Gamma_b|L_1|^2\right)L_3 = 0, \quad (36)$$

These equations are the same as those obtained in Eqs. (20), except the nonlinearity is effectively a factor 4/3 smaller, so that any solution requires higher power to excite it. As such, the solutions to Eqs. (36) are the same as those given in Eqs. (21)–(27) with the change that the factor $\sqrt{\kappa_g/\Gamma_b}$ is replaced by $\sqrt{4\kappa_g/3\Gamma_b}$. From Eqs. (31) and Eqs. (33) then a solution to the coupled-mode equations [Eqs. (9)] which couples from core to core is

$$\hat{\mathcal{F}}(\zeta,\tau) = \begin{pmatrix} L_1\cos(\kappa_c\zeta) \\ L_3\cos(\kappa_c\zeta) \\ iL_1\sin(\kappa_c\zeta) \\ iL_3\sin(\kappa_c\zeta) \end{pmatrix}, \quad (37)$$

where

$$L_1 = \alpha\sqrt{\frac{4\kappa_g}{3\Gamma_b}}\frac{1}{\Delta}\sin(\delta)e^{i\sigma}\mathrm{sech}(\theta - i\delta/2)e^{i\eta(\theta)},$$
$$L_3 = -\alpha\sqrt{\frac{4\kappa_g}{3\Gamma_b}}\Delta\sin(\delta)e^{i\sigma}\mathrm{sech}(\theta + i\delta/2)e^{i\eta(\theta)}, \quad (38)$$

and all other quantities are as defined in Eqs. (23)–(27).

As with the solutions in the preceding section, these solutions are strictly solitary waves, not solitons. However, unlike the other solutions, Eqs. (37) and (38) are not exact solutions of the coupled-mode equations [Eqs. (9)] since nonlinear terms proportional to $\exp(\pm 4i\kappa_c\zeta)$ were neglected in their derivation. It is seen from Eq. (37) that the solutions couple from core to core on a length scale of κ_c^{-1}; a pulse of the form given by Eqs. (38) launched into the twin-core-fiber rocking filter initially has all its power in one core and on traveling a distance $\zeta = \pi/(2\kappa_c)$ both polarization modes completely couple over to the other core and so on. Such behavior is nontrivial as one would expect the pulse to disperse due to intensity-dependent coupling effects and polarization dispersion. Also note that in the limit of small detuning δ and small velocity q the solutions in Eq. (37) reduce to those obtained in the nonlinear Schrödinger limit by PdS in their Eq. (12). In this limit it is seen that the solution is dominated by the beating of the $|1\rangle$ and $|3\rangle$ linear supermodes [see Eq. (16)].

The existence and stability of these switching solutions is verified in numerical simulations using the fields given in Eq. (37) along with Eq. (38) as input to the original coupled-mode equations [Eqs. (9)]. In these simulations the core-to-core coupling is taken to be given by $\kappa_c = 10\kappa_g$, which justifies the decision to omit the nonlinear terms proportional to $\exp(\pm 4i\kappa_c\zeta)$ in Eqs. (34). The initial conditions are such that fields are present in both polarization modes of one core only. The pulses are propagated over a distance of approximately 100 core-to-core coupling lengths for different velocity (q) and detuning (δ) parameters. Since the results obtained are qualitatively the same as those shown in Fig. 3 in the previous section [the only difference is that the peak power in each mode is a factor $\sqrt{4/3}$ larger] no results are presented here.

The effect of reducing the size of the core-to-core coupling κ_c was also investigated and it was found that even for κ_c a factor of 100 smaller there was no discernible difference in the results.

An important feature to note from the Fig. 3 is that the peak intensity of the fields is of order 300 W. The solution obtained in Eq. (12) of PdS typically has a peak intensity of the order of a few watts in the limit in which p and q are small. This bears out the claim made in this paper that the solutions given in Eq. (37) are generalizations of the solutions of PdS to high powers.

IV. STABILITY OF SOLUTIONS

In this section, the question of the stability of the solutions obtained in Sec. III is examined. First consider the solutions given in Eq. (29); in regard to the system of coupled-mode equations [Eqs. (9)], the *Ansatz* in Eq. (17) effectively reduces the phase space made up from $\mathcal{F}_{1x}$, $\mathcal{F}_{1y}$, $\mathcal{F}_{2x}$, and $\mathcal{F}_{2y}$ from eight (as the fields are complex) to four dimensions. An important question is whether the solutions [Eq. (29)] are stable to perturbations which would take them out of their subspace. No attempt has been made to give an analytic answer to this question; only numerical simulations were undertaken. A perturbation of the form

$$\mathcal{F}_{2x} = \mathcal{F}_{1x}(1+\epsilon), \qquad \mathcal{F}_{2y} = \mathcal{F}_{1y}(1+\epsilon) \tag{39}$$

was applied to the solutions given in Eq. (29). The results of the numerical simulations using Eq. (39) as input are discussed below. Next consider the solutions given in Eq. (37); in this case the perturbation given in Eq. (39) is not appropriate. One must go back to Eq. (35) and apply the perturbation at this stage. It can be shown that a perturbation $L_2 = L_1(1+\epsilon)$, $L_4 = L_3(1+\epsilon)$ in Eq. (38) indicates that the fields $\mathcal{F}_{nj}$ to be propagated down the fiber structure be modified from those given in Eq. (37) to

$$\begin{aligned} \mathcal{F}_{1x} &= L_1(1+\epsilon/2), \qquad \mathcal{F}_{2x} = -\epsilon L_1/2, \\ \mathcal{F}_{1y} &= L_3(1+\epsilon/2), \qquad \mathcal{F}_{2y} = -\epsilon L_3/2. \end{aligned} \tag{40}$$

Numerical simulations of the coupled-mode equations using Eq. (39) and Eq. (40) as input were performed for a variety of detunings (δ) and velocities (q) and perturbations were examined which were real or purely imaginary. It is found for both types of solutions that for detunings $\delta \lesssim \pi/2$ and for a wide range of velocites the pulses are stable to real perturbations as large as 25%, over distances of at least 250 core-to-core coupling lengths. It is also found that the behavior for imaginary perturbations is qualitatively the same as for real pertubations. The situation for larger-amplitude pulses is more complex and it unclear at this stage what conclusions can be drawn as regards their stability. Figure 4 shows the result of a simulation using Eq. (40) as input for a real perturbation $\epsilon = 0.2$. In this case the peak intensities in the x mode of each core have been added and similarly for the y mode in each core. This is done since in the unperturbed system this combination is constant as the pulse propagates down the fiber. It is clearly seen that, although the peak of the intensity undergoes periodic oscillations, it remains stable as it propagates. Overall, it seems that at least for smaller amplitude pulses $\delta \lesssim \pi/2$ they are quite stable to perturbations which take them out of their subspace.

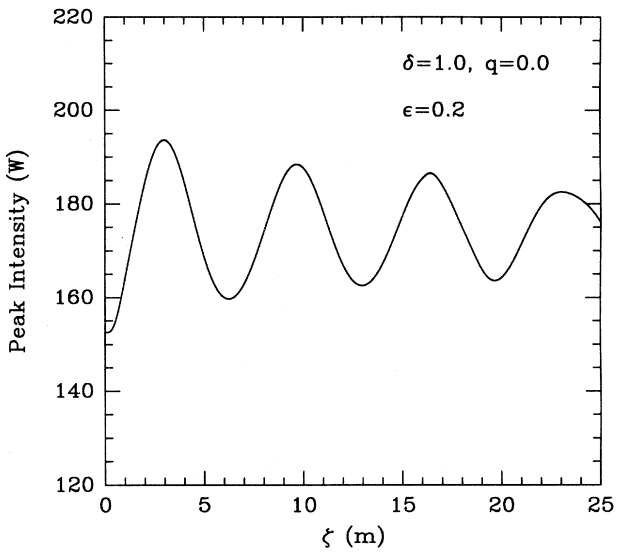

FIG. 4. Result of the numerical simulations of Eqs. (9) using the perturbed fields of Eq. (40) as input. The detuning, velocity, and size of the perturbation used are shown on the figure.

V. DISCUSSION AND CONCLUSION

In obtaining the solutions to the coupled-mode equations [Eqs. (9)] given by Eq. (29) and Eq. (37) the crucial step was the *Ansatz* given by either Eq. (17) or Eq. (35). One may ask whether these *Ansätze* are unique or do other possibilities exist? As far as the authors are aware, there appears to be only one other case, viz.,

$$\mathcal{F}_{1x} = -\mathcal{F}_{2x}, \qquad \mathcal{F}_{1y} = -\mathcal{F}_{2y}, \tag{41}$$

which also leads to a set of consistent coupled-mode equations which are identical to Eqs. (20), except κ_c is replaced by $-\kappa_c$. Now consider the relation of the solutions to the coupled-mode equations obtained in Eq. (29) and Eq. (37) to the gap structures shown in Fig. 2(b). The solutions of Eq. (29) correspond to a center wave vector $\kappa_c - \kappa_g < Q' < \kappa_c + \kappa_g$. To verify this is the case, one substitutes Eq. (29) along with Eqs. (22) into Eq. (8) and identifies the full wave-vector dependence. This outcome is effectively forced on one by use of the *Ansatz* given in Eq. (17). If on the other hand one used the *Ansatz* of Eq. (41), the solutions obtained from the resulting coupled-mode equations would correspond to pulses with center wave vector $-\kappa_c - \kappa_g < Q' < -\kappa_c + \kappa_g$, which corresponds to the stop gap on the left of Fig. 2(b). As regards the analysis of PdS, this alternative solution would correspond to taking $a_1 = 0$ rather than a_3 in their Eqs. (7). Finally note that, if the nonlinearity were negative rather than positive, the solutions to the coupled-mode equations would be such that the low-intensity limit corresponds to the right hand edge of the stop gaps shown in Fig. 2(b).

In the case of the solutions given by Eq. (37), analysis of the full wave-vector dependence obtained by substituting Eq. (37) along with Eqs. (38) into Eq. (8) shows

that wave vectors from both stop gaps shown in Fig. 2(b) are involved. This is to be expected, since in this case it is the beating at half the difference of the two center wave vectors (this difference is just $2\kappa_c$) that causes the coupling from core to core.

In conclusion, the properties of a twin-core, nonlinear in-line, resonant fiber rocking filter have been examined. It is shown that the system can have two stop gaps. The nonlinear coupled-mode equations [Eqs. (9)] which describe the system are solved in two special cases. In one case, exact solutions are found which represent a four-component solitary wave that propagates without degradation down the fiber as a whole, with equal power in each core. This solution is valid for a center wave vector anywhere in the stop gap indicated on the right of Fig. 2(b) and for any velocity between V_x and V_y. The other solution obtained represents a four-component solitary wave that periodically couples completely from core to core as it propagagtes down the fiber. In this case wave vectors from both gap regions shown in Fig. 2(b) are required. Both types of solution are found to propagate for hundreds of core-to-core coupling lengths without degradation and represent generalizations of the solutions obtained by PdS.

Finally, we note that the solutions presented here can be trivially extended to the case of contrapropagating pulses in a twin-core Bragg grating structure by simply interchanging the roles of time and space.

ACKNOWLEDGMENTS

This work was supported by the Australian Research Council. It was also supported by the Australian Photonics CRC.

[1] R. H. Stolen, A. Ashkin, W. Pleibel, and J. M. Dziedzic, Opt. Lett. **9**, 200 (1984).
[2] K. O. Hill, F. Bilodeau, B. Malo, and D. C. Johnson, Electron. Lett. **27**, 1548 (1991).
[3] S. Wabnitz, Opt. Lett. **14**, 1071 (1989).
[4] D. C. Psaila and C. M. de Sterke, Opt. Lett. **18**, 1905 (1993).
[5] C. Elachi, Proc. IEEE **64**, 1666 (1976).
[6] G. P. Agrawal, *Nonlinear Fiber Optics* (Academic, London, 1989), Chap. 7, p. 77.
[7] C. M. de Sterke and J. E. Sipe, Phys. Rev. A **42**, 550 (1990).
[8] T. Stefano, S. Wabnitz, and G. I. Stegeman, IEEE J. Quantum Electron. **25**, 1907 (1989).
[9] A. Yariv and P. Yeh, *Optical Waves in Crystals* (John Wiley & Sons, New York, 1984), Sec. 5.3.1.
[10] S. Wabnitz, S. Trillo, E. M. Wright, and G. I. Stegeman, J. Opt. Soc. Am. B, **8**, 602 (1991).
[11] H. A. Haus, *Waves and Fields in Optoelectronics* (Prentice-Hall, Englewood Cliffs, NJ, 1984).
[12] A. B. Aceves and S. Wabnitz, Phys. Lett. A **141**, 37 (1989).
[13] C. M. de Sterke, K. R. Jackson, and B. D. Robert, J. Opt. Soc. Am. B **8**, 403 (1991).